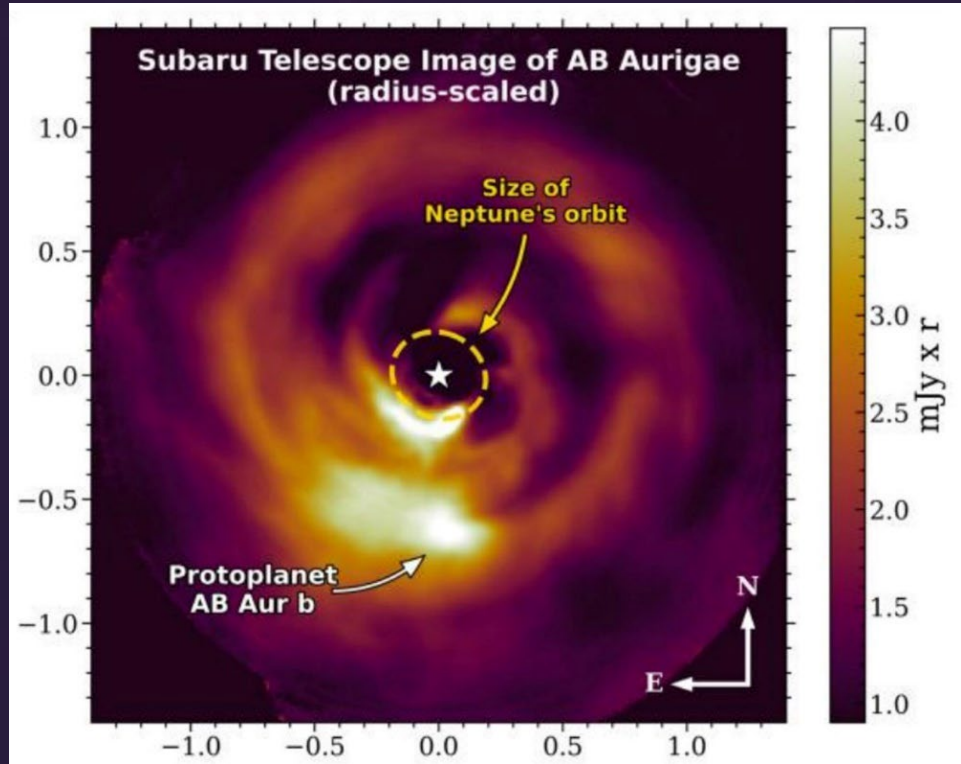


Introduction

Protoplanetary disks around young pre-main sequence stars (1-10 Myr) are known to be the sites of active planet formation. Such systems around Herbig Ae/Be stars are of particular interest because they are the predecessors to the systems where directly imageable planets are found. AB Aurigae is a well studied 2.4 M_{\odot} Herbig Ae star that is known to host an extensive protoplanetary disk, with numerous spirals ranging in scale between 20-500 au^{6,9}. It is also host to a recently identified protoplanet candidate, making it an excellent target to explore the characteristics of active sites of planet formation in NIR polarized light observations⁴.



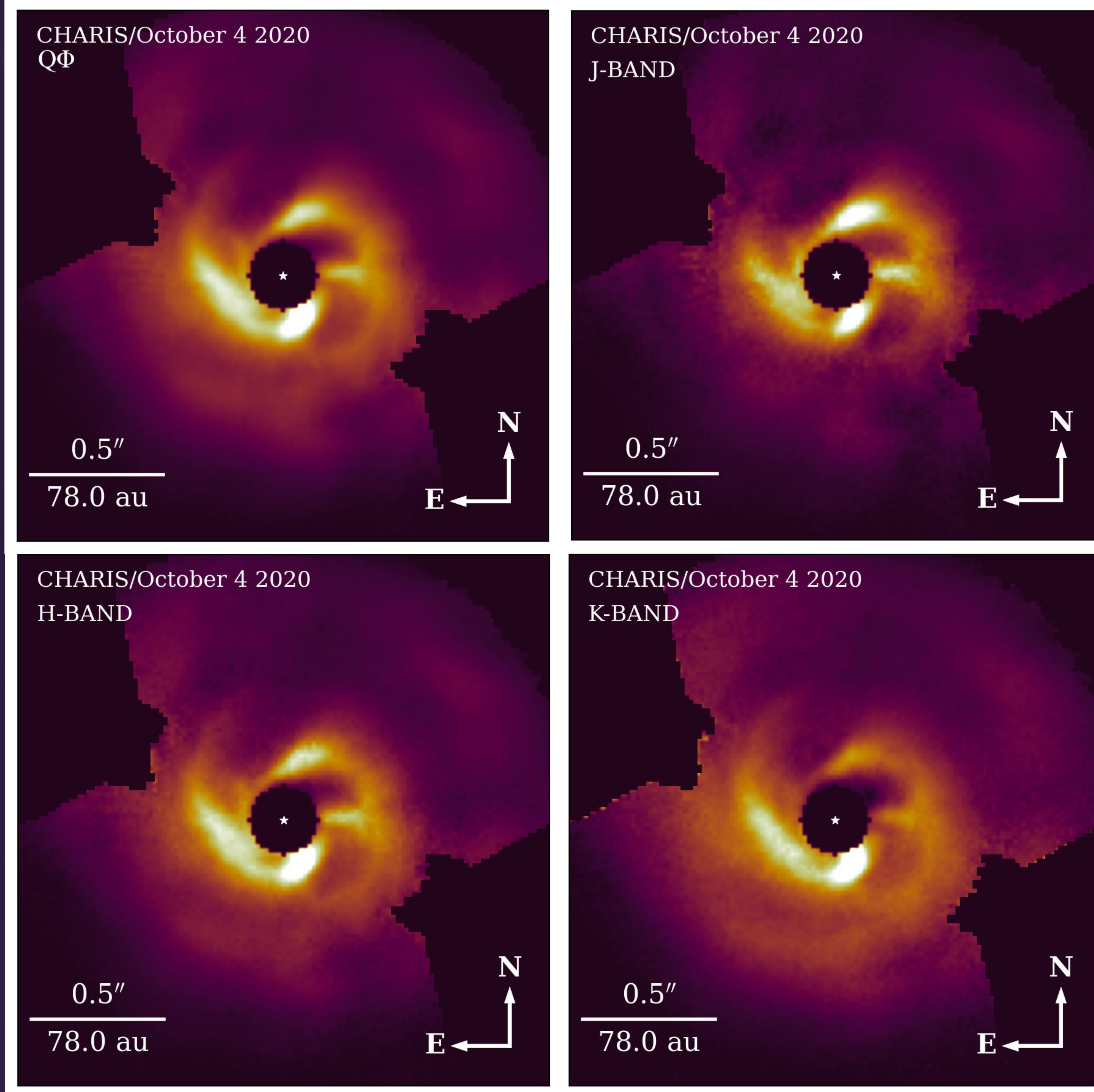
Polarimetric Differential Imaging (PDI) is unique among disk scattered light observing techniques because it doesn't pose the risk of distorting disk signals¹¹. This enables the identification of morphological features and the exploration of the physical properties of the dust in the surface layers of protoplanetary disks.

Observations & Reductions

73 exposures of AB Aurigae were taken on UT 2020 October 4 with SCEXAO/CHARIS in broadband PDI mode (1.1 -2.4 μm), amounting to a total exposure time of ≈ 74 minutes^{7,8}. Observations were then reduced and combined into the final data cubes with the standard PDI pathway of the CHARIS Data Processing Pipeline, which utilizes the double difference technique to produce the polarized light images (P.I., Q, U, U_{ϕ} , and Q_{ϕ})³.

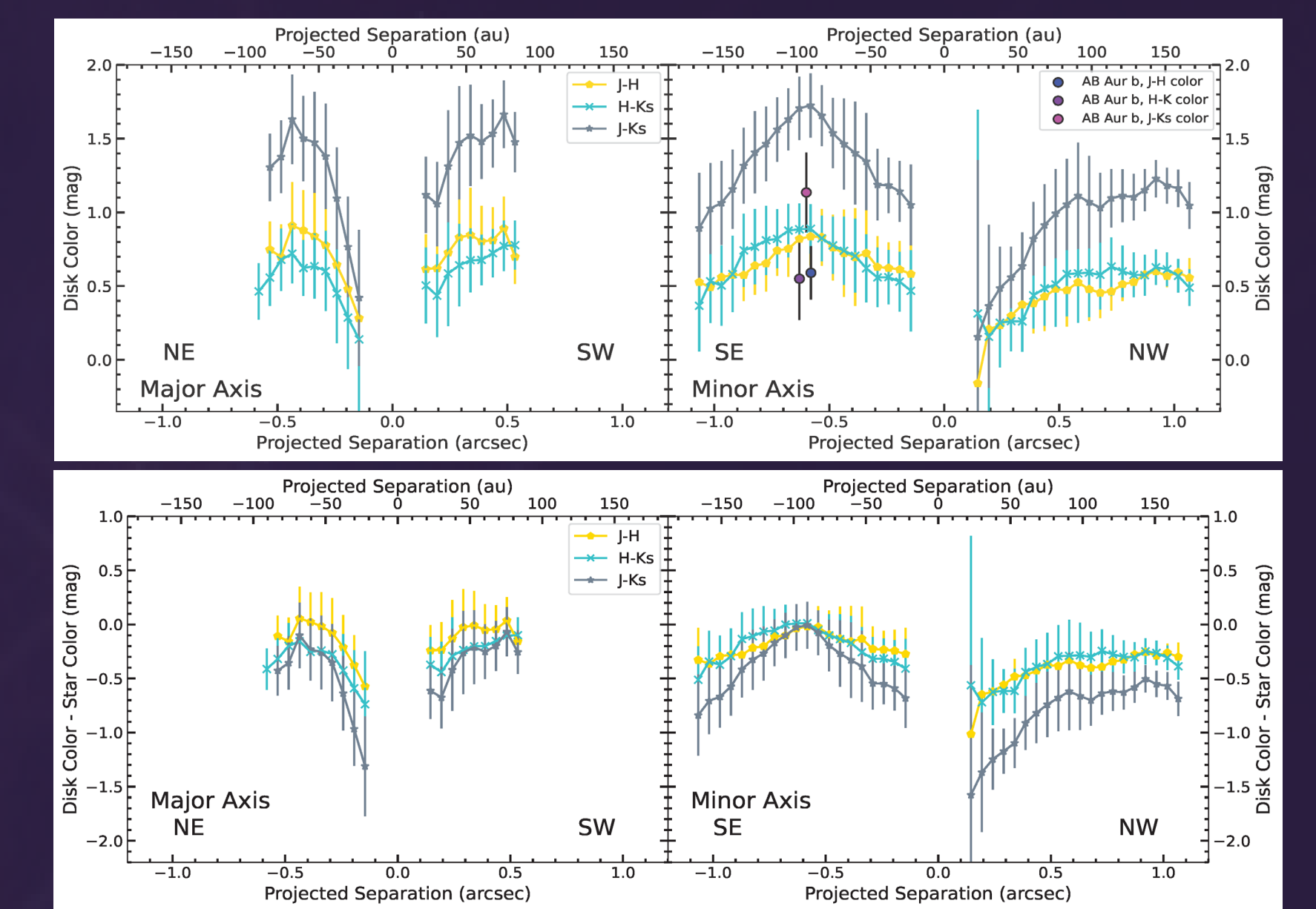
Table 1. AB Aurigae Observing Log

UT Date	Instrument	coronagraph	Seeing (")	Passband	λ (μm) ^a	t_{exp}	N_{exp}	ΔPA (")	Observing Strategy
20201004	SCEXAO/CHARIS	Lytot	0.6-0.8	JHK	1.16-2.39	60-69	73	80.0	PDI

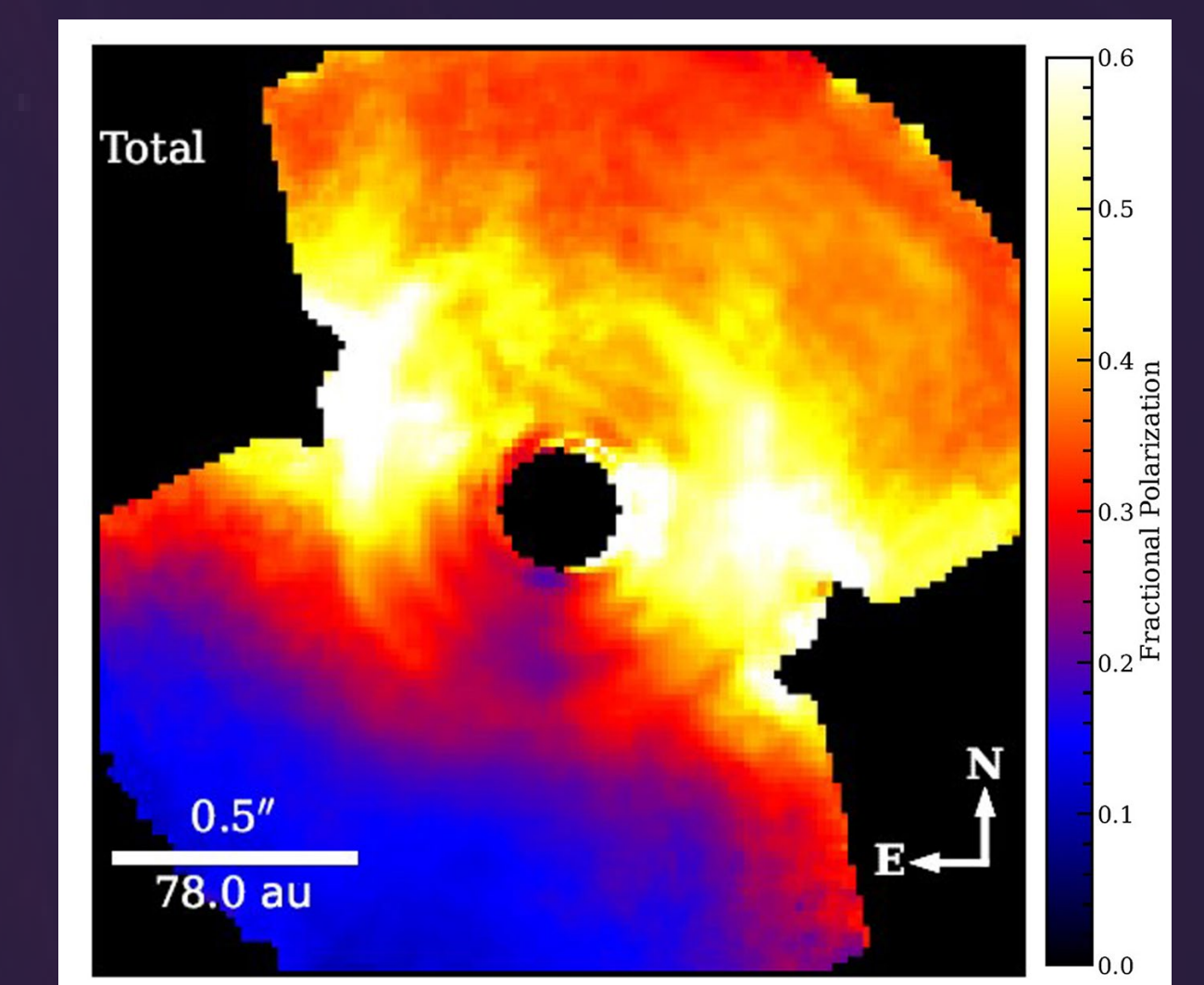


We were able to use the 22 wavelength channels encompassing the JHK passbands to determine that a number of the morphological features in AB Aur's disk display a wavelength dependence. The start of the eastern spiral, which was previously identified by Boccaletti et al. 2020, maintains an increased intensity ($\approx 1.5-1.7$ times the intensity of the rest of the spiral) and is consistently the brightest feature across the entire disk for all wavelength channels. We also see that the outer regions of the disk increase in intensity, becoming much closer to that of the spirals at longer wavelengths. There is no definitive concentrated signal near AB Aur b, consistent with previous reductions.

Analysis



We found that the intrinsic scattered-light color (i.e. the color when light from the AB Aur primary and unresolved sub-AU disk emissions were removed; see lower panel) of AB Aur's disk is grey/blue in contrast to its red apparent scattered-light color (upper panel).

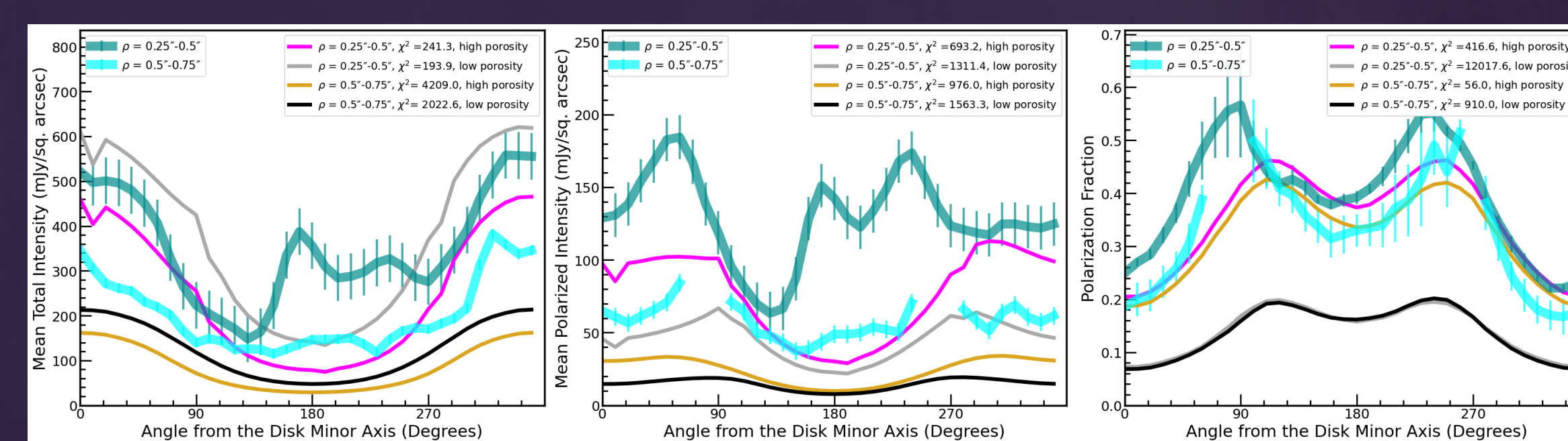


The polarization fraction across the disk displayed minimal wavelength dependence, with the forward scattering region consistently displaying the lowest polarization fraction of ≈ 0.15 , the back scattering region roughly doubling the fraction to $\approx 0.3-0.4$, and the major axis displaying the highest polarization fraction of ≈ 0.6 . The relatively high polarization fraction suggests that the surface regions of AB Aur's disk are populated by porous aggregates¹⁰.

Modeling

In order to explore the properties of the dust in the AB Aur system, we used the 3D Monte Carlo Radiative Transfer code MCFOST. Our best fit models required a composite source (9800 K Kurucz stellar atmosphere + 1950K free-free gas emission scaled to match the near-IR SED; previously implemented in Betti et al. 2022) to replicate both the previously observed 1-5 μm SED and our observed scattered light intensities. Following Perrin et al. 2009, we assumed the dust is comprised of astronomical silicates⁵ and used Mie theory to compute their scattering properties. Our models also assumed a number of fixed variables, primarily based on values established by previous works. These fixed values are listed below along with the source they are derived from (if applicable).

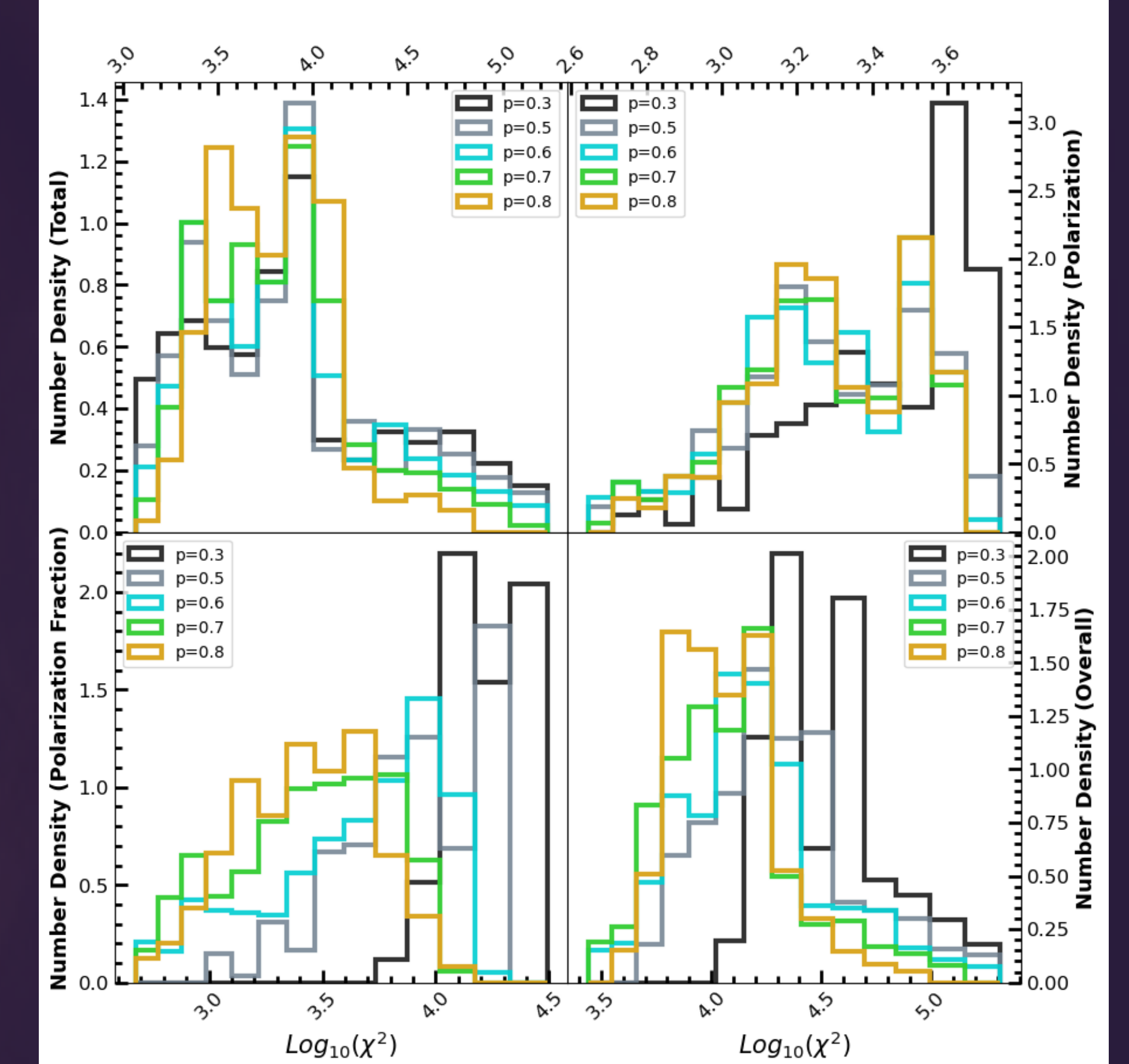
Fixed Parameters	Value	Reference
R_*	2.7 R_{\odot}	Currie et al. (2022)
T_{eff}^*	9800 K	Currie et al. (2022); Betti et al. (2022)
M_*	2.4 M_{\odot}	Currie et al. (2022)
Distance	155.9 pc	Gaia Collaboration (2022)
Surface density exponent, ϵ	1.0	Pinte et al. (2009); Perrin et al. (2009)
Reference radius, R_0	1 au	Pinte et al. (2009), this work
Disk flaring index, β	1.3	Perrin et al. (2009)
Disk inner radius, R_{in}	0.15 au	this work
Disk outer radius, R_{out}	300 au	this work
Disk Position Angle, PA	234°	Tang et al. (2017); Betti et al. (2022)
Maximum grain size, a_{max}	1 μm	this work, Currie et al. (2022)
Grain size power-law, p	-3.5	Pinte et al. (2009)



We varied the porosity of the dust (0.3-0.8), the disk's dust mass ($1e-5$ - $1e-4 M_{\odot}$), the reference scale height (0.0125-0.05), the minimum grain size (0.1-0.5), and the inclination angle (15-45°) across a coarse grid of 1,200 models. We then compared the models to previously collected total intensity data from Currie et al. 2022 as well as the polarized intensity and polarization fraction derived from this work by calculating the chi-square values for each model.

Our analysis showed that $p \geq 0.6$ is required to best match the observations, particularly the polarization fraction which strongly correlates with the porosity of the dust aggregates. While models with porosities $0.6 \leq p \leq 0.8$ fit well with the polarization fraction, our best first model overall and for the polarization fraction used $p=0.7$. See the azimuthal profiles above and the chi-square distributions to the right for further details on the effect varying the dust aggregates' porosities had.

Chi-Square Distributions (Porosity)



References

- Betti, S., Follette, K., Jorquera, S., et al. 2022, AJ, 163, 145
- Boccaletti, A., Di Folco, E., Pantin, E., et al., 2020, A&A, 637, L5
- Currie, T., Guyon, O., Lozi, J., et al. 2020, SPIE Conference Series, Vol. 11448, Ground-based and Airborne Instrumentation for Astronomy VII, ed. L. Schreiber, D. Schmidt, & E. Vernet, 114487H
- Currie, T., Lawson, K., Schneider, G., et al. 2022, Nature Astronomy, 6, 751
- Draine, B.T., & Lee H.M., 1984, ApJ, 285, 89
- Fukagawa, M., Hayashi, M., Tamura, M. et al. 2004, ApJL, 605, L53
- Groff, T. D., Chilcote, J., Kasdin, N.J., et al 2016, SPIE Conference Series, Vol. 9908, Ground-based and Airborne Instrumentation for Astronomy VI, 99090O
- Jovanovic, N., Martineche, F., Guyon, O., et al. 2015, PASP, 127, 890
- Perrin, M.D., Schneider, G., Duchene, G., et al. 2009, ApJL, 707, L132
- Tazaki, R., Tanaka, H., Muto, T., Kataoka, A., & Okuzumi, S., 2019, MNRAS, 485, 4951
- Van Holstein, R. G., Bos, S.P., Ruigrok, J. et al. 2020, SPIE Conference Series, Vol. 11447, Ground-based and Airborne Instrumentation for Astronomy VIII, ed. C.J. Evans, J.J. Bryant, & K. Motohara, 114475B

Summary

- Obtained images across 22 wavelength channels in J, H, and K passbands and determined the wavelength dependence of AB Aur's morphology.
- Determined that AB Aur's intrinsic scattered-light color is grey/blue.
- Found that the polarization fraction ranges from ≈ 0.15 in the forward scattering region to ≈ 0.6 along the major axis.
- The scattering properties of AB Aur's disk suggest the presence of higher porosity ($0.6 \leq p \leq 0.8$) dust aggregates.

Acknowledgement

This work was funded by the NASA/XRP program 80NSSC20K0252.